Evidence of Toroidally Localized Turbulence with Applied 3D Fields in the DIII-D Tokamak

R. S. Wilcox, M. W. Shafer, N. M. Ferraro, G. R. McKee, L. Zeng, T. L. Rhodes, J. M. Canik, C. Paz-Soldan, R. Nazikian, and E. A. Unterberg

Phys. Rev. Lett. **117**, 135001 — Published 21 September 2016

DOI: 10.1103/PhysRevLett.117.135001

Evidence of toroidally localized turbulence with applied 3D fields in the DIII-D tokamak

R. S. Wilcox,[1,*] M. W. Shafer,[1] N. M. Ferraro,[2] G. R. McKee,[3] L. Zeng,[4] T. L. Rhodes,[4] J. M. Canik,[1] C. Paz-Soldan,[5] R. Nazikian,[2] and E. A. Unterberg[1]

[1] *Oak Ridge National Laboratory, PO Box 2008, Oak Ridge, Tennessee 37831*
[2] *Princeton Plasma Physics Laboratory, Princeton, New Jersey 05764*
[3] *University of Wisconsin-Madison, Madison, Wisconsin 53706*
[4] *University of California Los Angeles, Los Angeles, California 90095*
[5] *General Atomics, San Diego, California 92121*

(Dated: September 2, 2016)

New evidence indicates that there is significant 3D variation in density fluctuations near the boundary of weakly 3D tokamak plasmas when resonant magnetic perturbations are applied to suppress transient edge instabilities. The increase in fluctuations is concomitant with an increase in the measured density gradient, suggesting that this toroidally localized gradient increase could be a mechanism for turbulence destabilization in localized flux tubes. Two-fluid magnetohydrodynamic simulations find that, although changes to the magnetic field topology are small, there is a significant 3D variation of the density gradient within the flux surfaces that is extended along field lines. This modeling agrees qualitatively with the measurements. The observed gradient and fluctuation asymmetries are proposed as a mechanism by which global profile gradients in the pedestal could be relaxed due to a local change in the 3D equilibrium. These processes may play an important role in pedestal and scrape-off layer transport in ITER and other future tokamak devices with small applied 3D fields.

The application of non-axisymmetric magnetic fields has been demonstrated as a mechanism for suppressing edge localized modes (ELMs) in high performance tokamak plasmas [1, 2]. While complete ELM suppression only occurs in certain ranges of edge safety factor q [3], density pumpout is a more consistent feature of DIII-D H-mode plasmas with applied 3D fields [4]. Recent experiments have linked both ELM suppression and density pumpout to resonant excitation of modes on magnetic surfaces with rational q values [5–7]. Understanding the physics of density pumpout has the potential to significantly improve the performance of fusion reactors if this confinement loss can be minimized while using 3D fields as an actuator for ELM and rotation control. The details of transport into the scrape-off layer with non-axisymmetric applied fields also have important implications for localized heat fluxes to the divertor, which has become a critical issue for ITER [8].

When 3D fields are applied and density pumpout occurs in DIII-D, the primary change to the plasma profiles is an increase in the electron density transport in the pedestal, where the density gradient is relaxed [2]. The electron temperature profiles are mostly unaffected, and the density gradient remains small everywhere inside the top of the pedestal.

Measured turbulence has previously been shown to respond rapidly to changes in applied 3D fields in DIII-D [9]. The increase in turbulence measured using beam emission spectroscopy (BES) following an increase in applied 3D field amplitude was shown to lead the change in density. This observation that the turbulence changes on a faster timescale than the particle transport suggests that the turbulence stability is responding directly to plasma equilibrium changes, rather than to changes in the global n=0 background gradients. The results presented here expand on this finding by correlating the measured fluctuations to the local stability of the underlying microturbulent modes.

In the DIII-D experiment examined here, the plasma had a toroidal field $B_T = 1.91$ T, normalized plasma beta $\beta_N = 2.0$, internal inductance $l_i = 0.9 - 1.0$, plasma current $I_P = 1.60$ MA, and 6 MW of injected neutral beam heating power. DIII-D has two rows of six in-vessel coils (I-coils) located above and below the outboard midplane of the device which apply small non-axisymmetric fields to the plasma. For this experiment, these coils were energized in an n=3 configuration, where the applied perturbation was predominantly pitch-resonant (even parity). The polarity of the current in the coils was flipped every 100 ms, effectively rotating the toroidal phase of the applied field by 60 degrees.

Fig. 1 presents the evolution of electron density and locally measured density fluctuations in a discharge with n=3 I-coil phase flips. An n=3 offset ramp was superimposed on periodic I-coil current polarity flips, as shown in Fig. 1(a). The asymmetric global density response with I-coil current is most likely due to intrinsic n=3 error fields. The D-α emission is then plotted in red using the right axis in Fig. 1 (a). Although ELMs are often triggered following the I-coil phase flips, most I-coil phases in the middle of the offset scan are ELM-free within ∼20 ms following the phase flip.

The line-averaged density from interferometry, $\overline{n}_e$, and pedestal density from Thomson scattering, $n_{e,ped}$, are

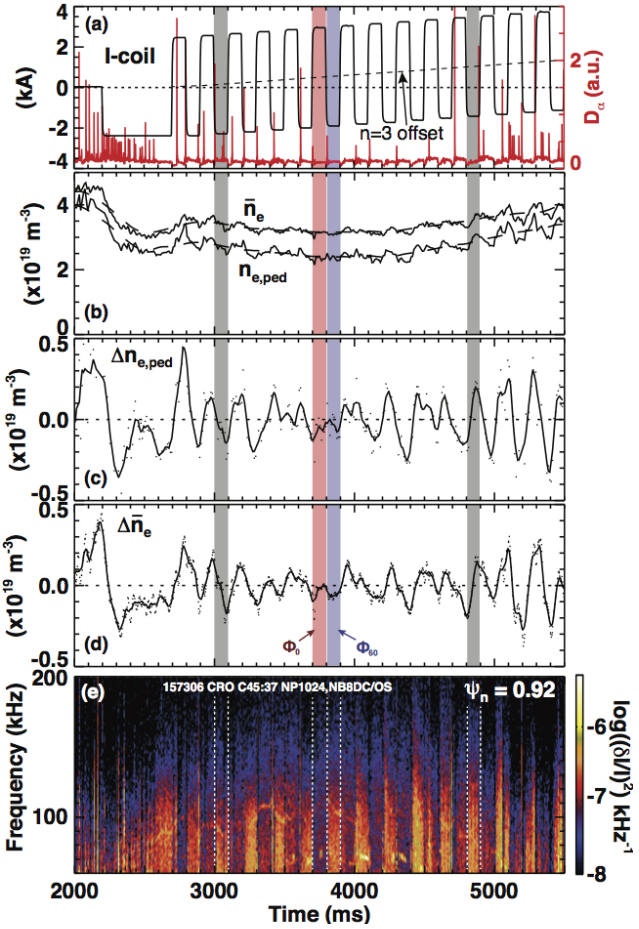

FIG. 1. Time traces from shot 157306 of (a) current from a sample I-coil (left axis, black), D-alpha emission (right axis, red), (b) line-averaged and pedestal density with dashed lines to indicate 200 ms moving averages, (c) pedestal density changes in time from Thomson scattering relative to the baseline over one period of I-coil phase flips, (d) line-averaged density changes from interferometer relative to the baseline and (e) spectral intensity of density fluctuations from BES.

given as a function of time in Fig. 1(b), with the 200 ms moving average of each shown as a dashed line, to give the running average over one period of I-coil phase flips. The time-varying component of pedestal and line-averaged density are then given in Fig. 1(c) and (d), respectively, each relative to their moving 200 ms average from the dashed lines in panel (b). These individual data points in time are then smoothed as well to give the line in each plot, which represents a 20 ms moving average.

During the beginning of the offset scan, as highlighted between 3000-3100 ms in Fig. 1, the density is decreasing when the given I-coil current is negative, indicating more pumpout than the average over an I-coil flip period. Further along in the offset scan, as highlighted at times 4800-4900 ms, the density increases (pumpout decreases) with similar phasing of the I-coils. Heating power and known particle sources were kept constant throughout the discharge time, so that any changes in the density here will be assumed to be due to particle transport changes. For I-coil phase flips in the middle of the scan, the global plasma response is similar between the two phases, suggesting that the effect of the n=3 error field on pumpout has been compensated at this point in the offset scan, and the effective amplitude of the total n=3 perturbation (applied plus intrinsic) is the same between the two phases. These time windows with similar global confinement between I-coil phases will be used to examine the difference between measurements in each phase as if the only difference between phases was the toroidal angle of each diagnostic measurement relative to the I-coils. Each diagnostic would then effectively be measuring different phases of the same plasma at a position rotated by 60 degrees toroidally, since the difference in the residual n=3 error field between the two toroidal phases is minimized and is not important to the n=0 transport. Error fields with other toroidal mode numbers are assumed to be small relative to the applied n=3 field. For the remainder of this paper, the I-coil phase when the given coil current is positive centered around t = 3750 ms will be referred to as ϕ_0 (highlighted in red in Fig. 1), and the phase when the I-coil current is negative centered around t = 3850 ms will be referred to as ϕ_{60} (blue in Fig. 1).

For the same discharge, the cross power spectrum of density fluctuations measured from two vertically displaced channels using beam emission spectroscopy (BES) [10] is plotted in Fig. 1(e) as a function of frequency and time for a channel with a collection area centered around $\psi_N = 0.92$, located poloidally at the outboard midplane and toroidally near the I-coil midpoint. BES is sensitive to density fluctuations for wavenumbers less than $\sim 2-3$ cm^{-1}. The pedestal turbulence wavenumber spectrum for the fluctuations here peaks near $k_\theta \rho_s \approx 0.15$. Intermittent coherent features are harmonics of lower frequency low-n core tearing modes not shown here.

BES measures fluctuations with consistently larger amplitudes in the ϕ_{60} toroidal phasing than in the ϕ_0 phase in and around the pedestal. Importantly, this relationship between the I-coil phase and fluctuation amplitude is consistent over the course of the n=3 offset scan, regardless of the globally-observed pumpout changes between phases. Changes to the pedestal E_r profiles correlate with the density pumpout characteristic, and therefore also appear to be unrelated to the fluctuation changes. This decoupling of the pedestal particle confinement (the density pumpout response) from the locally measured turbulence indicates that the turbulence may be localized toroidally relative to the applied perturbations.

Measurements of the pedestal density are made using the profile reflectometer system [11], which is located at the outboard midplane approximately 110 degrees toroidally from measurements made using the BES system. For an n=3 perturbation, the density profiles are therefore expected to be qualitatively similar to those at

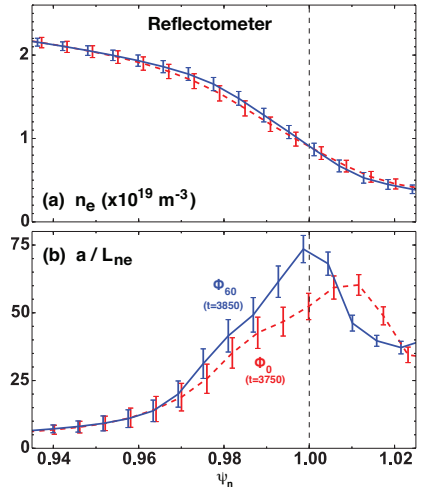

FIG. 2. (a) Electron density and (b) normalized inverse density gradient scale length a/Lne as measured by the reflectometer, in the high-BES-turbulence ϕ_{60} phase (blue, solid) and low-BES-turbulence ϕ_0 phase (red, dashed).

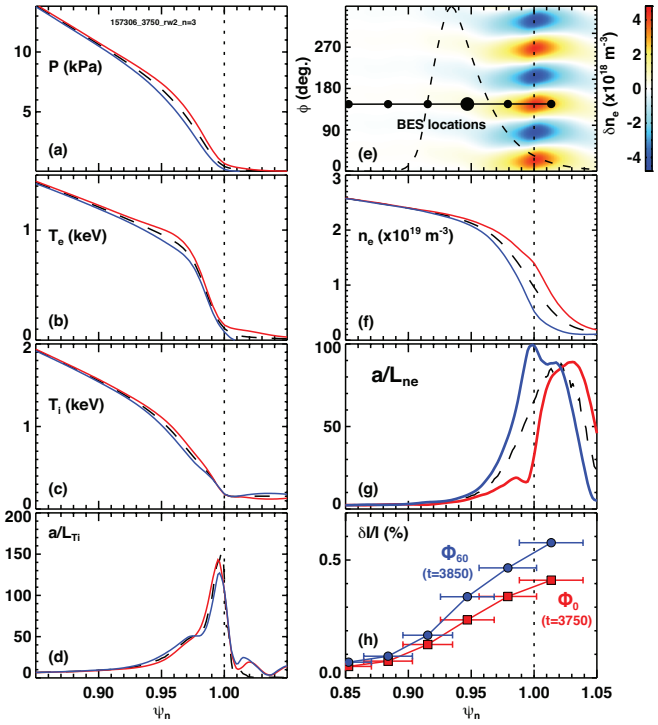

FIG. 3. M3D-C1 modeled profiles of (a) total pressure, b) electron temperature, (c) ion temperature, (d) ion temperature gradient scale length, (e) n=3 electron density perturbations as a function of toroidal angle, along with the BES measurement locations and an example diagnostic sampling range, (f) electron density and (g) electron density gradient scale length, all at the outboard midplane for the I-coil phases ϕ_0 (red) and ϕ_{60} (blue). (h) Integrated BES fluctuations measured for the two phases.

the location of the BES measurements in Fig. 1(e). The experimentally observed electron density and normalized density gradient scale length, $a/L_{n_e} = a\nabla\ln(n_e)$ where a is the minor radius, are plotted in Fig. 2 for the two I-coil phases ϕ_0 and ϕ_{60}, as measured by the reflectometer. The inverse density gradient scale length is measured to be larger for ϕ_{60}, which is the phase where BES observes larger fluctuation amplitudes. If it is assumed that the applied n=3 field is the dominant non-axisymmetric structure, then the BES and reflectometer measurements are nearly effectively co-located, suggesting that the density gradient increase in this toroidal phase may be a mechanism for the destabilization of a microturbulent mode in the flux tubes where the gradient is larger. The errorbars given here are determined based on the standard deviation of the density and its gradient in each of the frequency sweeps of the reflectometer source.

Mechanisms have been proposed in which the turbulence stability is modified by small deviations from axisymmetry through the local geometric shaping quantities of the magnetic surfaces, such as curvature, flux expansion and local magnetic shear [12, 13]. In the case presented here, these quantities are calculated using VMEC [14] to be modified only slightly, less than 1% each. Making any standard assumption of the relationship between geometric shaping quantities and the resulting fluctuations [15], the local 3D geometric shaping would therefore be expected to play a subdominant role in directly affecting the linear microstability.

The M3D-C1 code is used to calculate the time-independent perturbed equilibrium with a linear resistive two-fluid model [16]. The modeled radial profiles of total pressure, electron temperature and ion temperature are plotted in Fig. 3(a), (b), and (c) respectively at the BES measurement location for the two I-coil phases where the n=3 error field is corrected. Contours in red correspond to ϕ_0, and contours in blue correspond to ϕ_{60}. The modeled 3D distortions to the radial density profiles are then shown in Fig. 3(e). These density perturbations are plotted as a function of normalized flux and toroidal angle, poloidally located at the outboard midplane. The measurement locations of the BES diagnostic are shown as black dots, with the diagnostic response function of a single BES channel given by a dashed line to indicate the radial sampling range. The BES measurement is toroidally located near a peak of the modeled density perturbation.

The normalized density gradient scale length a/L_{n_e} calculated from the M3D-C1 equilibrium is then given in Fig. 3(g), and shows significant variation between the two toroidal phases. The modeled normalized ion temperature gradient scale length $a/L_{T_i} = a\nabla\ln(T_i)$, plotted in Fig. 3(d), exhibits much less toroidal variation than a/L_{n_e}. This indicates that the change in a/L_{n_e} is due to density changes *within the flux surface*, as opposed to toroidally varying flux surface deformation, which would affect all profile gradients similarly. Although the mag-

nitude of density changes measured by the reflectometer from Fig. 2 are not as large as those modeled by the linearized M3D-C1 simulations, the qualitative gradient changes between the phases are similar.

Finally, the integrated high frequency density fluctuations from BES (> 85 kHz) are plotted in Fig. 3(h) for several spatial channels across the pedestal region. The errorbars represent the half-width of the diagnostic response functions. The toroidal phase in which the modeled density gradient scale length is increased corresponds to the I-coil phase where the BES measures larger density fluctuations, which is again consistent with the proposed mechanism for turbulence destabilization.

Single-fluid M3D-C1 calculations did not reproduce the spatial variation of the density gradient within the flux surfaces, and further testing indicated that perpendicular ion rotation was important to establishing this pressure gradient within a flux surface. A perturbed electrostatic potential enables the formation of the parallel density and pressure gradient within the flux surface. The density iso-surfaces are shifted by the fluid velocity, but the magnetic surfaces shift with the E×B velocity. Since the difference of these terms is the ion diamagnetic velocity, the density gradient can develop spatial variation within a flux surface in the pedestal region, where this term is large. These perturbed density structures are elongated helically along the magnetic field lines. Other devices have measured helically perturbed potential profiles with applied 3D fields [17], and these perturbations may be measurable in the cases presented here as well, although the effect is expected to be second order compared to the large radial potential gradients in the pedestal.

M3D-C1 has been previously shown to agree quantitatively with edge displacements in DIII-D [18]. The modeled electron temperature and density profiles from the M3D-C1 simulations are compared with measurements at the Thomson scattering location for this discharge in Fig. 4. Although the linearized model may be overpredicting the 3D deformations to the temperature iso-surfaces at the top of the pedestal, the displacement of the surfaces agrees well with the measurement across most of the steep gradient region, where the turbulence observations here are focused. The modeled density in the pedestal matches the Thomson scattering measurement within errorbars. However, the phase of the modeled density is such that the perturbations within a flux surface are much smaller at the Thomson scattering location than at the outboard midplane, where the reflectometer measurements are made. Based on the Thomson scattering data and M3D-C1 simulations, flow screening of resonant fields is strong and there are no signs of islands in the steep gradient region.

The mode structure of the underlying instability need not be localized to the outboard midplane, but this location is simply where the relevant diagnostics are. Wherever the unstable mode is localized poloidally and

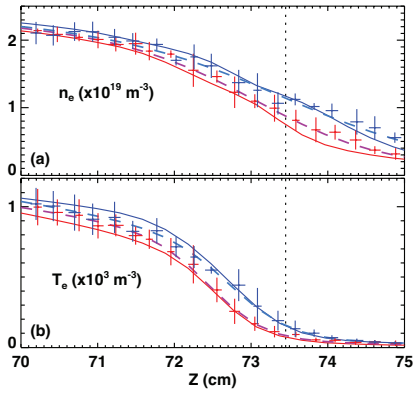

FIG. 4. (a) Electron density and (b) temperature in and around the pedestal at the Thomson scattering measurement location, as measured by Thomson scattering (crosses) and modeled by M3D-C1 (solid lines) in the two I-coil phases ϕ_0 (t=3750 in red) and ϕ_{60} (t=3850 in blue). Dashed lines indicate the profile fit to the Thomson scattering data.

toroidally on a flux surface, the non-axisymmetric density structures and the fluctuations will both extend along the flux tubes to the outboard midplane where they are observed. Therefore, both the field-aligned density perturbations and fluctuations should be consistent along the same flux bundles, regardless of where the microinstability is sourced. Gyrokinetic simulations for an axisymmetric DIII-D equilibrium have shown that both a trapped electron mode (TEM) and kinetic ballooning mode are unstable in the pedestal, and the TEM can exhibit a mode structure that is localized at the top and bottom of the torus [19].

There are also two Doppler backscattering (DBS) systems in DIII-D measuring density fluctuations in the pedestal with approximate poloidal wavenumber $k_\theta \approx 3$ cm^{-1} which are located at the outboard midplane, separated toroidally 180 degrees from each other [20]. Each of these is modeled to be near a null in the n=3 equilibrium density perturbation phase, so that neither would be expected to show large differences in fluctuation magnitudes in either phase. One of these systems measures similar fluctuation amplitudes in both I-coil phases, as expected, while the second observes a dependence with I-coil phase that matches the BES system. It is speculated that n≠3 error fields play a role in the observations by the second system, which would be expected to measure nearly zero difference in fluctuations between phases for the modeled n=3 perturbations that are dominant elsewhere. Uncorrected n=2 error fields are estimated to contribute the equivalent of ≤ 1 kA of I-coil current [6], while uncorrected n=1 error fields are smaller due to the standard application of n=1 error field correction.

The application of 3D fields might also increase the saturated, non-linear turbulence by reducing the zonal flow response [21]. This is beyond the scope of this work,

but zonal flow changes and the linear stability changes presented here are not mutually exclusive. However, any changes to the zonal flows would lead to n=0 changes to the turbulence, where the measurements shown here demonstrate a toroidal dependence to the fluctuations.

This paper has presented the first evidence of toroidal variation of turbulence with relatively small applied 3D fields in a tokamak. M3D-C1 simulations as well as measurements using the reflectometer indicate an increase in the density gradient scale length in the flux tubes where turbulence is increased, as measured by BES. This occurs in the same region where the global density gradient is relaxed when 3D fields are applied. Because particle and energy transport is generally dominated by turbulent fluxes in tokamaks, this suggests a possible link between these fluctuations and density pumpout, which is an important unexplained phenomenon in high performance tokamak plasmas. Further measurements or simulations would be required to relate the density fluctuations observed here to their associated transport fluxes. Localization of the heat and particle fluxes to the divertor in ITER could also be impacted by these fluxes. This work underscores the importance of including 3D effects in this and other gyrokinetic transport modeling, even in plasmas with only small deviations from axisymmetry.

Work supported in part by the US DOE under contracts DE-AC05-00OR22725, DE-AC02-09CH11466, DE-FG02-08ER54999, DE-FG02-08ER54984, DE-FC02-04ER54698.

* wilcoxrs@ornl.gov

[1] T. E. Evans, R. A. Moyer, K. H. Burrell, M. E. Fenstermacher, I. Joseph, A. W. Leonard, T. H. Osborne, G. D. Porter, M. J. Schaffer, P. B. Snyder, P. R. Thomas, J. G. Watkins, and W. P. West, Nature Physics **2**, 419 (2006).

[2] M. R. Wade, R. Nazikian, J. S. deGrassie, T. E. Evans, N. M. Ferraro, R. A. Moyer, D. M. Orlov, R. J. Buttery, M. E. Fenstermacher, A. M. Garofalo, M. A. Lanctot, G. R. McKee, T. H. Osborne, M. A. Shafer, W. M. Solomon, P. B. Snyder, W. Suttrop, A. Wingen, E. A. Unterberg, and L. Zeng, Nuclear Fusion **55**, 023002 (2015).

[3] O. Schmitz, T. E. Evans, M. E. Fenstermacher, M. Lehnen, H. Stoschus, E. A. Unterberg, J. W. Coenen, H. Frerichs, M. W. Jakubowski, R. Laengner, C. L. Lasnier, S. Mordijck, R. A. Moyer, T. H. Osborne, H. Reimerdes, D. Reiter, U. Samm, B. Unterberg, and the DIII-D and TEXTOR teams, Nuclear Fusion **52**, 043005 (2012).

[4] T. E. Evans and the DIII-D Team, Plasma and Fusion Research **7**, 2402046 (2012).

[5] C. Paz-Soldan, R. Nazikian, S. R. Haskey, N. C. Logan, E. J. Strait, N. M. Ferraro, J. M. Hanson, J. D. King, M. J. Lanctot, R. A. Moyer, M. Okabayashi, J.-K. Park, M. W. Shafer, and B. J. Tobias, Physical Review Letters **114**, 105001 (2015).

[6] C. Paz-Soldan, N. C. Logan, M. J. Lanctot, J. M. Hanson, J. D. King, R. J. L. Haye, R. Nazikian, J.-K. Park, and E. J. Strait, Nuclear Fusion **55**, 083012 (2015).

[7] R. Nazikian, C. Paz-Soldan, J. D. Callen, J. S. deGrassie, D. Eldon, T. E. Evans, N. M. Ferraro, B. A. Grierson, R. J. Groebner, S. R. Haskey, C. C. Hegna, J. D. King, N. C. Logan, G. R. McKee, R. A. Moyer, M. Okabayashi, D. M. Orlov, T. H. Osborne, J.-K. Park, T. L. Rhodes, M. W. Shafer, P. B. Snyder, W. M. Solomon, E. J. Strait, and M. R. Wade, Physical Review Letters **114**, 105002 (2015).

[8] A. Loarte, G. Huijsmans, S. Futatani, L. R. Baylor, T. Evans, D. M. Orlov, O. Schmitz, M. Becoulet, P. Cahyna, Y. Gribov, A. Kavin, A. S. Naik, D. Campbell, T. Casper, E. Daly, H. Frerichs, A. Kischner, R. Laengner, S. Lisgo, R. Pitts, G. Saibene, and A. Wingen, Nuclear Fusion **54**, 033007 (2014).

[9] G. R. McKee, Z. Yan, C. Holland, R. J. Buttery, T. E. Evans, R. A. Moyer, S. Mordijck, R. Nazikian, T. L. Rhodes, O. Schmitz, and M. R. Wade, Nuclear Fusion **53**, 113011 (2013).

[10] G. R. McKee, R. J. Fonck, M. W. Shafer, I. U. Uzun-Kaymak, and Z. Yan, Review of Scientific Instruments **81**, 10D741 (2010).

[11] L. Zeng, W. A. Peebles, E. J. Doyle, T. L. Rhodes, N. Crocker, X. Nguyen, C. W. Wannberg, and G. Wang, Review of Scientific Instruments **85**, 11D843 (2014).

[12] T. M. Bird and C. C. Hegna, Nuclear Fusion **53**, 013004 (2013).

[13] T. M. Bird and C. C. Hegna, Physics of Plasmas **21**, 100702 (2014).

[14] S. P. Hirshman, W. I. Van Rij, and P. Merkel, Computer Physics Communications **43**, 143 (1986).

[15] H. E. Mynick, P. Xanthopoulos, and A. H. Boozer, Physics of Plasmas **16**, 110702 (2009).

[16] N. M. Ferraro, Physics of Plasmas **19**, 056105 (2012).

[17] G. Spizzo, N. Vianello, R. B. White, S. S. Abdullaev, M. Agostini, R. Cavazzana, G. Ciaccio, M. E. Puiatti, P. Scarin, O. Schmitz, M. Spolaore, D. Terranova, and RFX and TEXTOR Teams, Physics of Plasmas **21**, 056102 (2014).

[18] N. M. Ferraro, T. E. Evans, L. L. Lao, R. A. Moyer, R. Nazikian, D. M. Orlov, M. W. Shafer, E. A. Unterberg, M. R. Wade, and A. Wingen, Nuclear Fusion **53**, 073042 (2013).

[19] D. P. Fulton, Z. Lin, I. Holod, and Y. Xiao, Physics of Plasmas **21**, 042110 (2014).

[20] W. A. Peebles, T. L. Rhodes, J. C. Hillesheim, L. Zeng, and C. Wannberg, Review of Scientific Instruments **81**, 10D902 (2010).

[21] H. Sugama and T.-H. Watanabe, Physics of Plasmas **13**, 012501 (2006).